Published in final edited form as:
Invest Ophthalmol Vis Sci. 2009 March ; 50(3): 1344–1349. doi:10.1167/iovs.08-2703.

Three-Dimensional Optical Coherence Tomography (3D-OCT) Image Enhancement with Segmentation-Free Contour Modeling C-Mode

Hiroshi Ishikawa[1,2], **Jongsick Kim**[1,2], **Thomas R. Friberg**[1,2], **Gadi Wollstein**[1], **Larry Kagemann**[1,2], **Michelle L. Gabriele**[1,2], **Kelly A. Townsend**[1], **Kyung R. Sung**[1], **Jay S. Duker**[3], **James G. Fujimoto**[4], and **Joel S. Schuman**[1,2]

[1]UPMC Eye Center, Eye and Ear Institute, Ophthalmology and Visual Science Research Center, Department of Ophthalmology, University of Pittsburgh School of Medicine, Pittsburgh, Pennsylvania

[2]Department of Bioengineering, Swanson School of Engineering, University of Pittsburgh, Pittsburgh, Pennsylvania

[3]New England Eye Center, Tufts Medical Center, Tufts University School of Medicine, Boston, Massachusetts

[4]Department of Electrical Engineering and Computer Science and Research Laboratory of Electronics, Massachusetts Institute of Technology, Cambridge, Massachusetts

Abstract

Purpose—To develop a semiautomated method to visualize structures of interest (SoIs) along their contour within three-dimensional, spectral domain optical coherence tomography (3D SD-OCT) data, without the need for segmentation.

Methods—With the use of two SD-OCT devices, the authors obtained 3D SD-OCT data within 6 × 6 × 1.4-mm and 6 × 6 × 2-mm volumes, respectively, centered on the fovea in healthy eyes and in eyes with retinal pathology. C-mode images were generated by sampling a variable thickness plane semiautomatically modeled to fit the contour of the SoI. Unlike published and commercialized methods, this method did not require retinal layer segmentation, which is known to fail frequently in the presence of retinal pathology. Four SoIs were visualized for healthy eyes: striation of retinal nerve fiber (RNF), retinal capillary network (RCN), choroidal capillary network (CCN), and major choroidal vasculature (CV). Various SoIs were visualized for eyes with retinal pathology.

Results—Seven healthy eyes and seven eyes with retinal pathology (cystoid macular edema, central serous retinopathy, vitreoretinal traction, and age-related macular degeneration) were imaged. CCN and CV were successfully visualized in all eyes, whereas RNF and RCN were visualized in all healthy eyes and in 42.8% of eyes with pathologies. Various SoIs were successfully visualized in all eyes with retinal pathology.

Corresponding author: Gadi Wollstein, UPMC Eye Center, Eye and Ear Institute, Ophthalmology and Visual Science Research Center, Department of Ophthalmology, University of Pittsburgh School of Medicine, 203 Lothrop Street, Suite 835, Pittsburgh, PA 15213; wollsteing@upmc.edu.

Presented in part at the annual meeting of the Association for Research in Vision and Ophthalmology, Fort Lauderdale, Florida, April 2008.

Disclosure: **H. Ishikawa**, None; **J. Kim**, None; **T.R. Friberg**, None; **G. Wollstein**, Carl Zeiss Meditec (F), Optovue (F); **L. Kagemann**, None; **M.L. Gabriele**, None; **K.A. Townsend**, None; **K.R. Sung**, None; **J.S. Duker**, None; **J.G. Fujimoto**, Optovue (I, C), Carl Zeiss Meditec (P); **J.S. Schuman**, Carl Zeiss Meditec (P)

Conclusions—The proposed C-mode contour modeling may provide clinically useful images of SoIs even in eyes with severe pathologic changes in which segmentation algorithms fail.

Medical imaging has long played a critical role in diagnosing and assessing various pathologic conditions. In the past decade alone, along with the rapid evolution of computer technologies, various new imaging modalities have been introduced. These provide three-dimensional (3D) image datasets and are proving themselves to be clinically useful. One of the main advantages afforded with a 3D image dataset is flexible image visualization capability. One can slice the target tissue in any arbitrary plane, allowing clinicians to study abnormalities from various vantage points (e.g., sagittal, coronal, and horizontal sections).

Optical coherence tomography (OCT) was developed in 1991 and was commercially introduced to ophthalmology in 1996.[1,2] First-generation OCT instruments provided a 2D cross-sectional view of the human retina at a microscopic resolution (10 μm) in vivo. Because of its noncontact and noninvasive imaging capabilities, OCT quickly became an indispensable clinical tool for assessing retinal abnormalities, including the leading causes of blindness: age-related macular degeneration, diabetic retinopathy, and glaucoma.[2–5] New techniques based on spectral/Fourier domain detection have achieved approximately 50× increases in imaging speeds.[6–8] With its fast axial imaging rate, SD-OCT has enabled us to obtain relatively high-density 3D cube data of the human retina within a reasonable scan time (e.g., 27 kHz sampling or 200 × 200 × 1024 samples in approximately 1.48 seconds; Fig. 1a). Although conventional C-mode images along the planes perpendicular to the scanning axis provide an interesting perspective, interpretation of such C-mode images is not intuitive because multiple different retinal layers are sliced in the same view given the natural spherical curvature of the eye (Fig. 1b).[9,10] In addition to this natural tissue curvature, an eye moves along the *z*-axis on a microscopic scale even within the short scanning time, leading to a distorted 3D SOCT image dataset (Fig. 1c).

A commercial SD-OCT (Cirrus HD-OCT; Carl Zeiss Meditec, Dublin, CA; software version 3.0) was used to solve this problem because it provides the capability of sampling the OCT data set along a segmented layer (internal limiting membrane [ILM], retinal pigment epithelium [RPE], or fitted curve to the RPE) with arbitrary thickness. This segmented C-mode method contains only structures in the segmented layer(s) and provides an improved view compared with conventional C-mode, which intersects multiple tissue planes (Fig. 2). Unfortunately, the quality of the segmented C-mode image depends on the quality of the automated segmentation algorithm performance. The deterioration of segmentation algorithm performance in the presence of retinal pathology is well described (Fig. 3).[11,12]

The purpose of this study was to develop a method to easily isolate structures of interest (SoIs) while generating C-mode images in a semiautomated fashion and to describe the clinical applications of such a technique.

Methods

Seven healthy eyes and seven eyes with retinal pathology (cystoid macular edema, central serous retinopathy, vitreoretinal traction, age-related macular degeneration) were enrolled by retrospectively reviewing the scanning record at the University of Pittsburgh Medical Center Eye Center. Healthy eyes had no history or evidence of intraocular surgery, retinal pathology or glaucoma, or refractive errors of less than 8 D and normal-appearing ONHs. All healthy eyes had normal results of comprehensive ocular examination and automated perimetry findings within normal limits.

The macular region was scanned on all eyes using either of two SD-OCT devices, an ultrahigh-resolution research prototype of our own design and Cirrus OCT (Carl Zeiss Meditec). The

ultrahigh-resolution research prototype had 3.0- to 3.5-μm axial image resolution and an imaging speed of 25,000 axial scans per second, whereas the Cirrus OCT (Carl Zeiss Meditec) had 5-μm resolution and a speed of 27,000 axial scans per second. All imaging was performed through undilated pupils. Institutional review board and ethics committee approval were obtained for the study, and informed consent was obtained from all subjects. This study followed the tenets of the Declaration of Helsinki and was conducted in compliance with the Health Insurance Portability and Accountability Act.

Image Acquisition

Prototype SD-OCT

Three-dimensional cube OCT data were obtained with a raster-scanning pattern centered at the fovea and consisting of 180 frames of horizontal linear B-scan with 501 A-scan lines (501 × 180 × 1024 [width × height × depth] voxels within 6 × 6 × 1.4 mm, scan time 3.84 seconds). Images with poor signal level (subjectively assessed) were discarded. In addition, images with detectable eye motion throughout the scan—larger than one vessel diameter or a major distortion of the foveal region in OCT fundus images—were discarded. Raw spectral domain signal data were exported and processed into universal time-domain intensity data format with a software program of our own design.

Cirrus OCT

Three-dimensional cube OCT data were obtained using the macular cube 200 × 200 scan pattern, which consists of 200 frames of a horizontal linear B-scan with 200 A-scan lines (200 × 200 × 1024 voxels within 6 × 6 × 2 mm; scan time, 1.48 seconds). Images with signal strength (SS) less than 8 were considered of poor quality and were discarded. In addition, images with detectable eye motion were discarded based on the same OCT fundus image criteria described. OCT scan raw data (processed by Cirrus system software, version 3.0; Carl Zeiss Meditec) were exported and processed into universal time-domain intensity data format with the same software to ensure that 3D cube OCT data obtained with either of the devices were further processed in the same manner.

C-Mode Image Generation

C-mode images were generated by a contour modeling method, sampling a variable thickness plane semiautomatically modeled to fit the contour of the SoI. This interactive, semiautomated process was performed with a software program of our own design, as described below:

1. User places multiple anchor points, which are connected with a spline-interpolated line, on one of the horizontal sections (Fig.4). Each user input (moving/deleting an existing anchor point or adding a new anchor point) triggers a C-mode image update, providing real-time interaction to the user for easy manipulation.
2. User repeats step 1 on a vertical section (Fig. 5).
3. User repeats steps 1 and 2 to get a satisfactory outcome contour-modeled C-mode image. Modeled contours in horizontal and vertical sections are interlinked so that changes can be made in any section but are automatically and instantaneously applied to the entire image. More anchor points are typically needed on a vertical section because of eye motion along the z-axis during imaging (Fig. 6). At the end, a complex 3D contour model of SoI is generated internally.

Image Evaluation

Four SoIs were targeted for visualization: striation of retinal nerve fiber (RNF), retinal capillary network (RCN), choroidal capillary network (CCN), and major choroidal vasculature (CV).

C-mode images for each of these four SoIs were generated with conventional (flat plane), segmented (conventional adaptive threshold segmentation of ILM, RNFL, and RPE),[11] and contour-modeling methods. Incomplete patchy visualization of an SoI was considered a failure. In addition, various SoIs (e.g., cystoid lesion, drusen) were visualized for eyes with retinal pathologies.

Results

CCN and CV were successfully visualized in all eyes; RNF and RCN were visualized in 100% of healthy eyes and 42.8% of eyes with abnormalities (Figs. 7–10, generated from the same 3D cube data acquired using the prototype SD-OCT). Primary reasons for unsuccessful visualization of RNF and RCN in eyes with abnormalities were inconsistent signal level and difficult-to-model contour of the diseased SoIs. Conventional C-mode images showed multiple layers in the same slice, making it harder to comprehend the target structure than segmented and contour-modeling images. Although there was no subjective difference in image quality between segmented and contour-modeling images for CCN and CV (Figs. 9, 10), the contour-modeling images visualized SoIs better did than the segmented images for RCN because the contour line was different from that of ILM and RPE (Fig. 8). The contour-modeling method also showed better RNF images than did the segmented method (Fig. 7).

Various SoIs were successfully visualized in all eyes with retinal abnormalities that could not be fully comprehended by examining individual cross-sectional images (Figs. 11-14). A subject with cystoid macular edema had a cystoid lesion with an interesting vascular network (Fig. 11). Another with central serous retinopathy had serous detachment in the foveal region with a highly reflective structure, likely corresponding to the region of leakage causing the detachment (Fig. 12). A subject with wet ARMD had clear demarcation lines of multiple drusen with marked elevation of the fovea (Fig. 13). An eye with substantial vitreoretinal traction had retinal folds at the level of the ILM centered at the traction point (Fig. 14).

Discussion

The ideal method for displaying C-mode images is to show only the target layer or structure. Using the segmentation information should, therefore, be a natural path leading to ideal C-mode images. However, as described, automatically segmenting pathologic structures is still a difficult task. This generates the need for an interim solution to easily visualize specific SoIs to take full advantage of the information embedded in 3D OCT data sets.

The present results show a clear advantage of contour-modeling C-mode over conventional C-mode. All nonspecific SoIs, except RCN, were visualized equally well with contour-modeling and segmented C-mode because ILM and RPE segmentation worked well on healthy samples. RCN has a contour line different enough from that of the ILM and the RPE that contour-modeling C-mode outperformed the segmented C-mode even without segmentation failure.

In subjects with abnormalities, ILM and RPE segmentation failed frequently, which made segmented C-mode images difficult to interpret. On the other hand, the contour-modeling method provided consistently good-quality C-mode images, even with complicated pathologic structures.

A limitation of contour modeling is its requirement for user interaction, but this approach is a viable solution given the current status of automated segmentation. This method typically requires only three or four anchor points in a horizontal section because horizontal raster scan sections are acquired more quickly and show less eye motion-related distortion than vertical sections. Ten to 30 anchor points are typically required in vertical sections, depending on the frequency of *z*-direction eye motion during imaging. Given that the contour line between the

anchors is automatically smoothed by spline interpolation and the C-mode image is updated in real time (fully interactive), the overall time required for a trained operator to process one 3D OCT dataset is 1 to 2 minutes.

When segmentation is successful, it is easier to start from a segmented plane than a flat plane and to further modify the contour model to suit the clinician's needs. Having a hybrid option may facilitate faster and easier processing. This feature has yet to be implemented and evaluated.

In conclusion, the proposed contour-modeling C-mode method may provide clinically useful images of intraretinal structures even in eyes with severe pathologic changes in which segmentation algorithms fail.

Acknowledgments

Supported in part by National Institutes of Health contracts R01-EY13178–08, R01-EY11289–23, and P30-EY08098–22, The Eye and Ear Foundation (Pittsburgh, PA), and unrestricted grants from Research to Prevent Blindness, Inc. (New York, NY).

References

1. Huang D, Swanson EA, Lin CP, et al. Optical coherence tomography. Science 1991;254(5035):1178–1181. [PubMed: 1957169]
2. Schuman JS, Pedut-Kloizman T, Hertzmark E, et al. Reproducibility of nerve fiber layer thickness measurements using optical coherence tomography. Ophthalmology 1996;103(11):1889–1898. [PubMed: 8942887]
3. Hee MR, Puliafito CA, Wong C, et al. Optical coherence tomography of macular holes. Ophthalmology 1995;102(5):748–756. [PubMed: 7777274]
4. Schuman JS, Hee MR, Arya AV, et al. Optical coherence tomography: a new tool for glaucoma diagnosis. Curr Opin Ophthalmol 1995;6(2):89–95. [PubMed: 10150863]
5. Hee MR, Baumal CR, Puliafito CA, et al. Optical coherence tomography of age-related macular degeneration and choroidal neovascularization. Ophthalmology 1996;103(8):1260–1270. [PubMed: 8764797]
6. Cense B, Nassif NA, Chen TC, et al. Ultrahigh-resolution high-speed retinal imaging using spectral-domain optical coherence tomography. Opt Express 2004;12:2435–2447. [PubMed: 19475080]serial online
7. Wojtkowski M, Srinivasan V, Fujimoto JG, et al. Three-dimensional retinal imaging with high-speed ultrahigh-resolution optical coherence tomography. Ophthalmology 2005;112(10):1734–1746. [PubMed: 16140383]
8. Srinivasan VJ, Wojtkowski M, Witkin AJ, et al. High-definition and 3-dimensional imaging of macular pathologies with high-speed ultrahigh-resolution optical coherence tomography. Ophthalmology 2006;113(11):2054.e1–e14. [PubMed: 17074565]
9. Cucu RG, Podoleanu AG, Rogers JA, et al. Combined confocal/en face T-scan-based ultrahigh-resolution optical coherence tomography in vivo retinal imaging. Opt Lett 2006;31(11):1684–1686. [PubMed: 16688261]1
10. Alam S, Zawadzki RJ, Choi S, et al. Clinical application of rapid serial Fourier-domain optical coherence tomography for macular imaging. Ophthalmology 2006;113(8):1425–1431. [PubMed: 16766031]
11. Ishikawa H, Stein DM, Wollstein G, et al. Macular segmentation with optical coherence tomography. Invest Ophthalmol Vis Sci 2005;46(6):2012–2017. [PubMed: 15914617]
12. Chan A, Duker JS, Ishikawa H, et al. Quantification of photoreceptor layer thickness in normal eyes using optical coherence tomography. Retina 2006;26(6):655–660. [PubMed: 16829808]

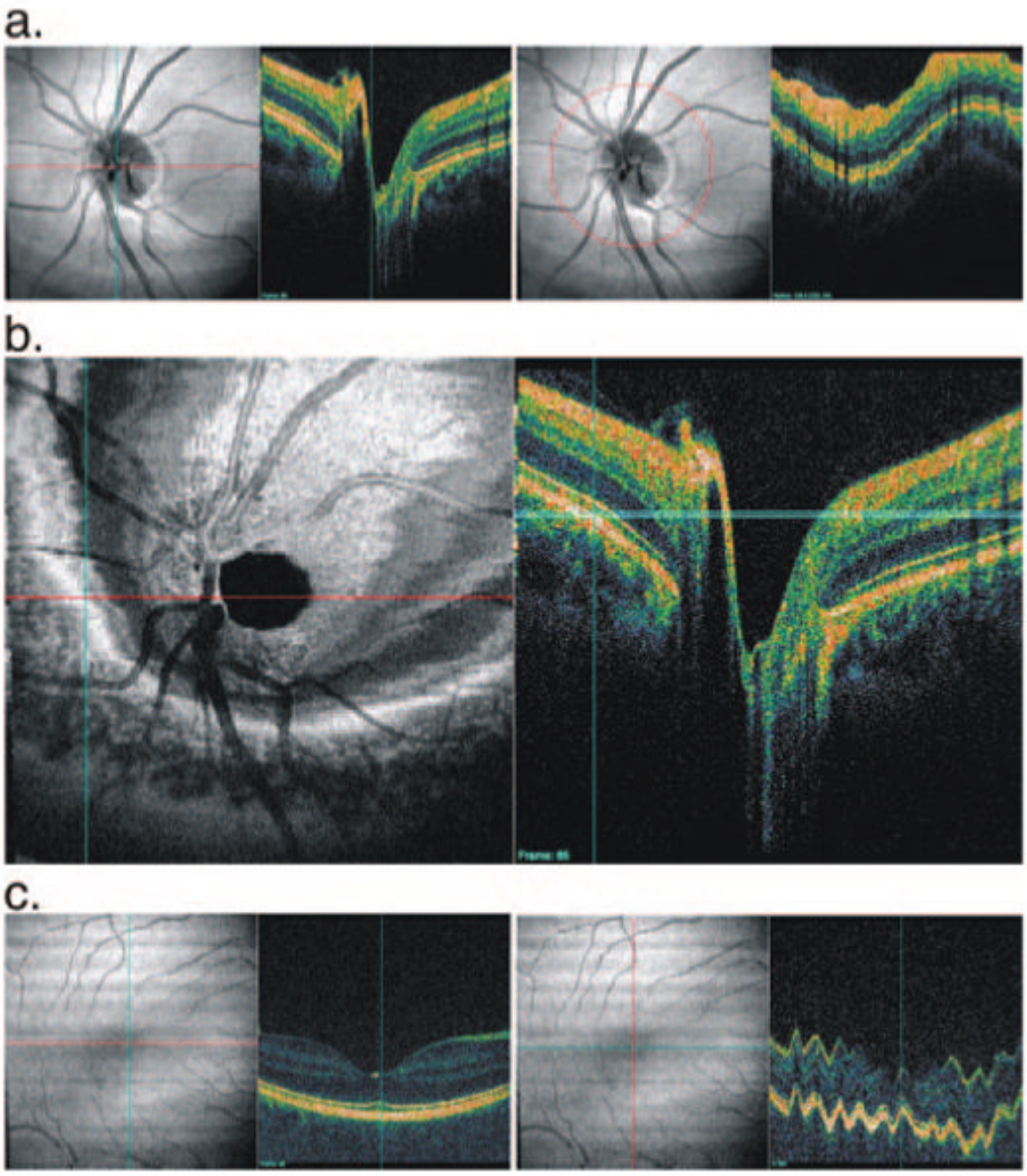

Figure 1.

(**a**) SD-OCT sample images showing (*left*) horizontal slice and (*right*) circular slice. (**b**) Conventional C-mode view of human retina obtained by prototype SD-OCT unit (501 × 180 × 1024 samplings in a 6 × 6 × 1.4-mm region). C-mode image (*left*) shows a concentric circular texture and a distorted view of the target layer structure that are caused by slicing multiple different layer structures in the retina with a straight line (*light blue band, right*). (**c**) A 3D SD-OCT data set that may appear to have minimal eye motion on viewing of a horizontal section (*left*) shows significant axial eye motion along a vertical section (*right*).

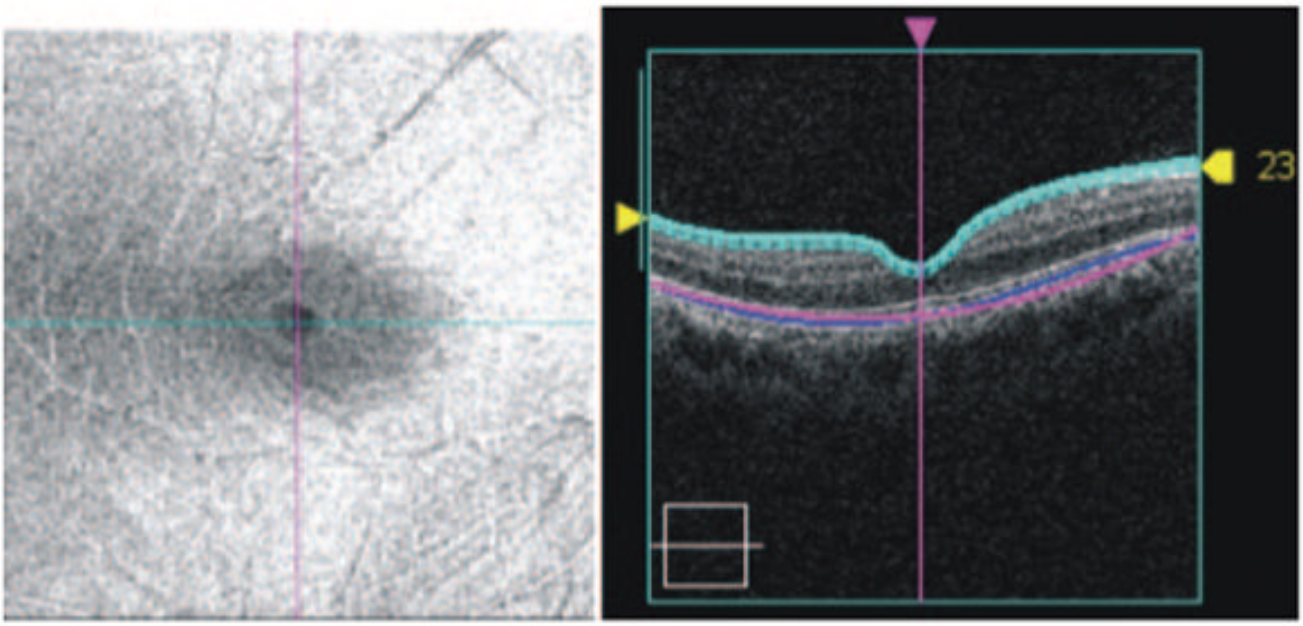

Figure 2.
OCT segmented C-mode image. C-mode image (*left*) shows a projection from the ILM (*right, within light blue lines*) with a thickness of 23 μm.

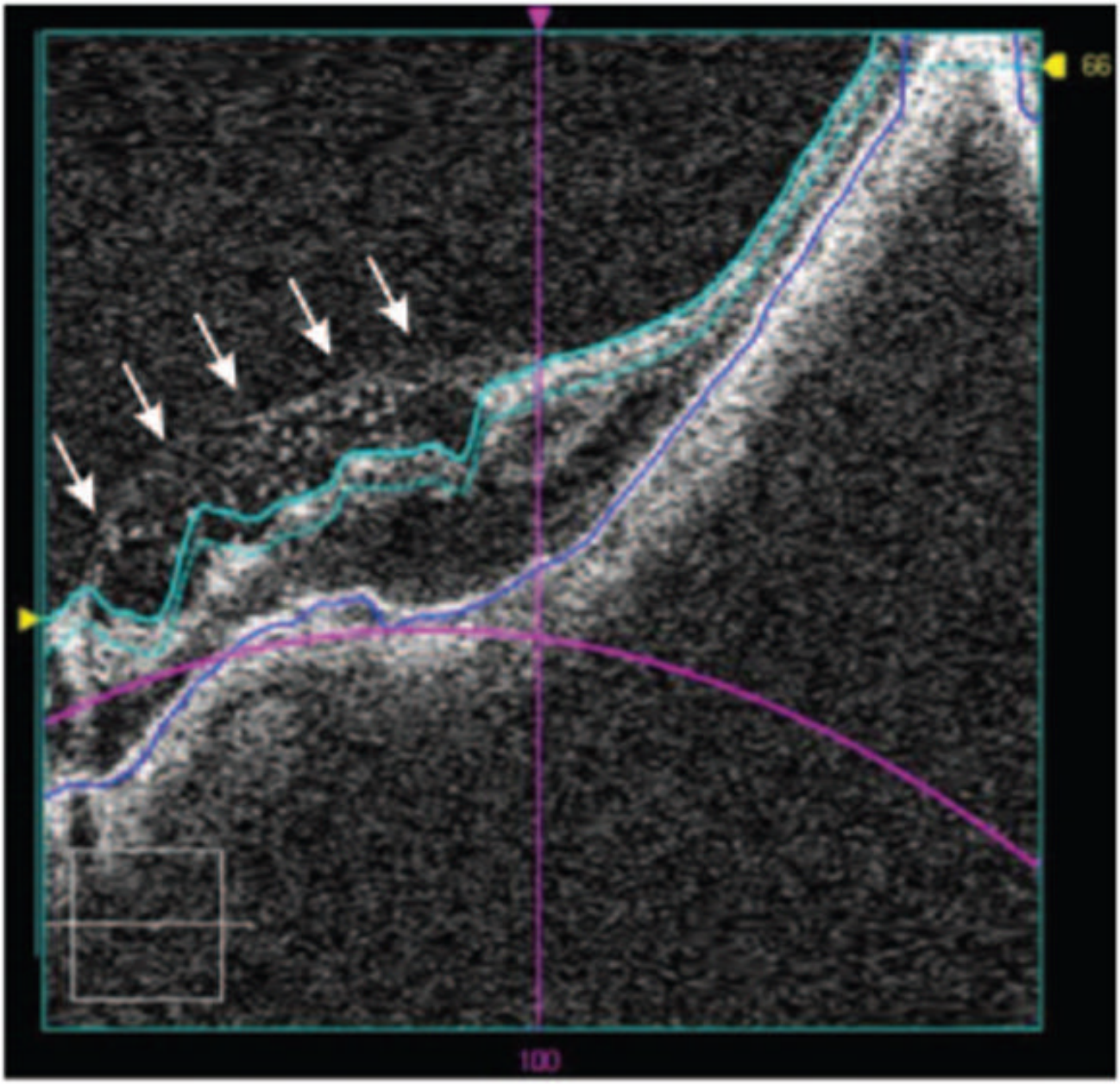

Figure 3.
Segmentation error sample. The segmented ILM border (*top, light blue line*) is not following the ILM properly at the cystic lesion (*arrows*) because of unusual retinal structure and poor signal quality. The smoothed fitted line (*magenta*) of the RPE also shows a tissue border definition that has no correlation with the detected RPE border (*blue line*).

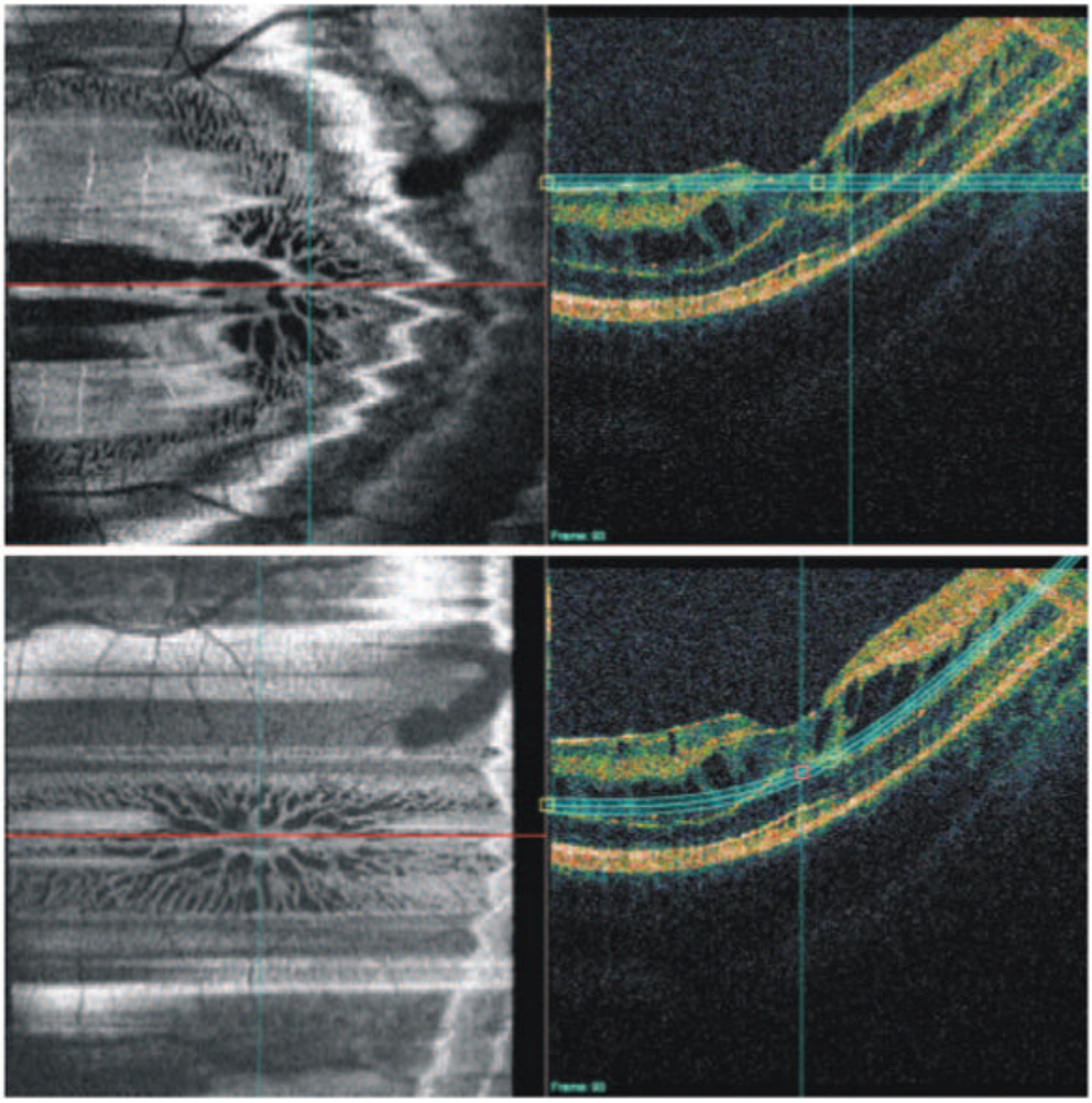

Figure 4.
Cystic changes in the macular region. Multiple layers are represented in the initial C-mode image (*top left*), making interpretation difficult. After adjusting the locations of three anchor points on a single B-mode tomogram (*horizontal section, bottom right*; *red line* on *left* defines the retinal location of the single B-mode tomogram on the *right*), the C-mode image (*bottom left*) starts to show a more precise image. Note the variability of intensity along several *horizontal* frames because of *z*-axis offset irregularities in the *vertical* section.

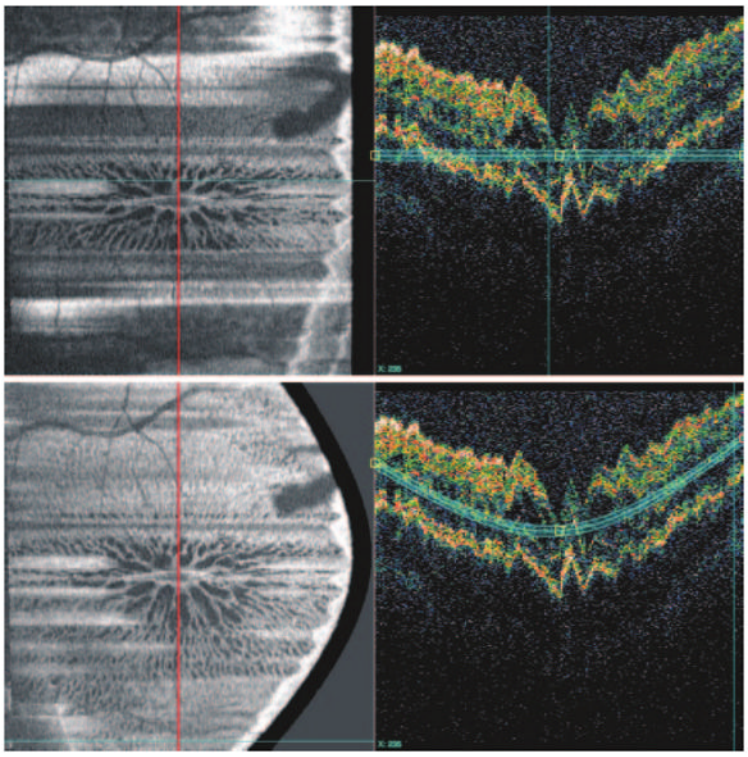

Figure 5.
Switching to a *vertical* section (along the *red line, left*), the C-mode image (*top*) stays the same as the C-mode image from Figure 4 (*bottom*) because no contour modeling on the vertical section has been performed. Note the jagged contour on the vertical section caused by eye motion along *z*-axis during imaging. After adjusting three anchor locations in a single B-mode tomogram (*bottom right*), most of the horizontal artifact on the C-mode image is resolved (*bottom left*).

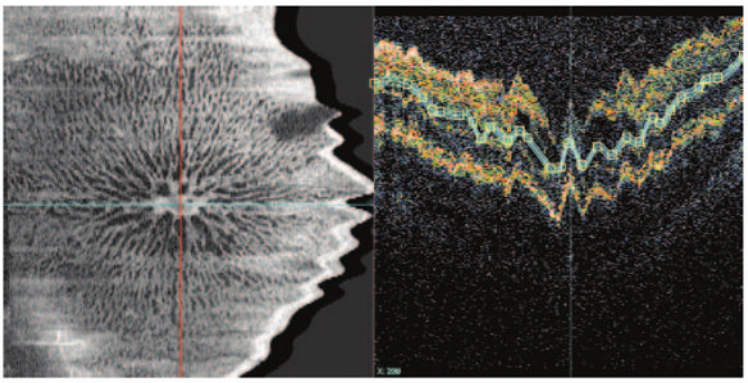

Figure 6.
Further refining the vertical contour modeling using multiple anchor points revealed the full extent of the cystic changes.

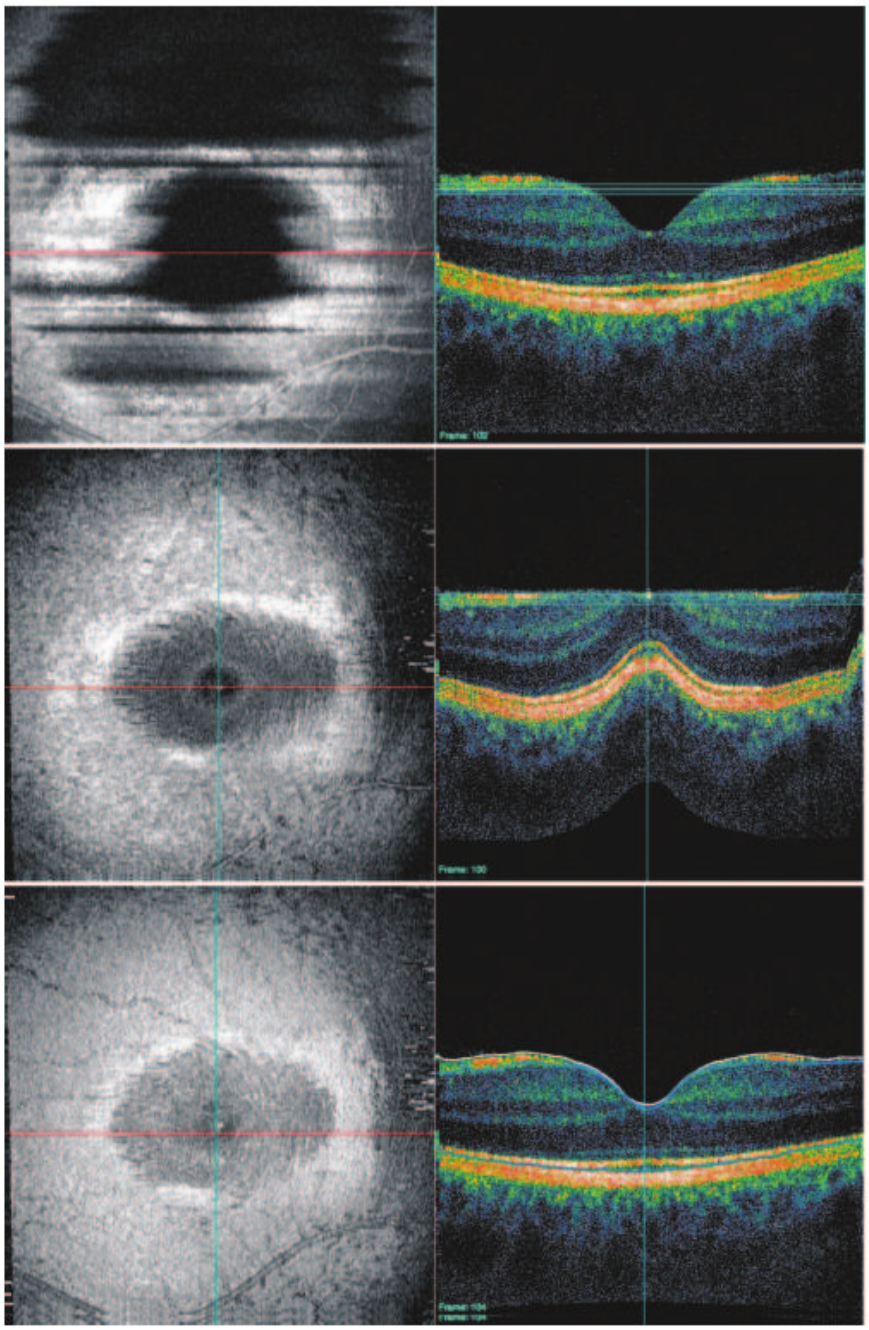

Figure 7.
RNF striation. Conventional C-mode (*top*) is marred with a mixture of multiple structures (dark area represents the vitreous cavity). Segmented C-mode (*middle*) shows the striation near the fovea but is not as detailed as the contour modeling C-mode (*bottom*). Note that this middle image was obtained with our prototype SD-OCT unit and that the image for the segmented C-mode was first flattened to the segmented ILM, resulting in a distorted cross-sectional image.

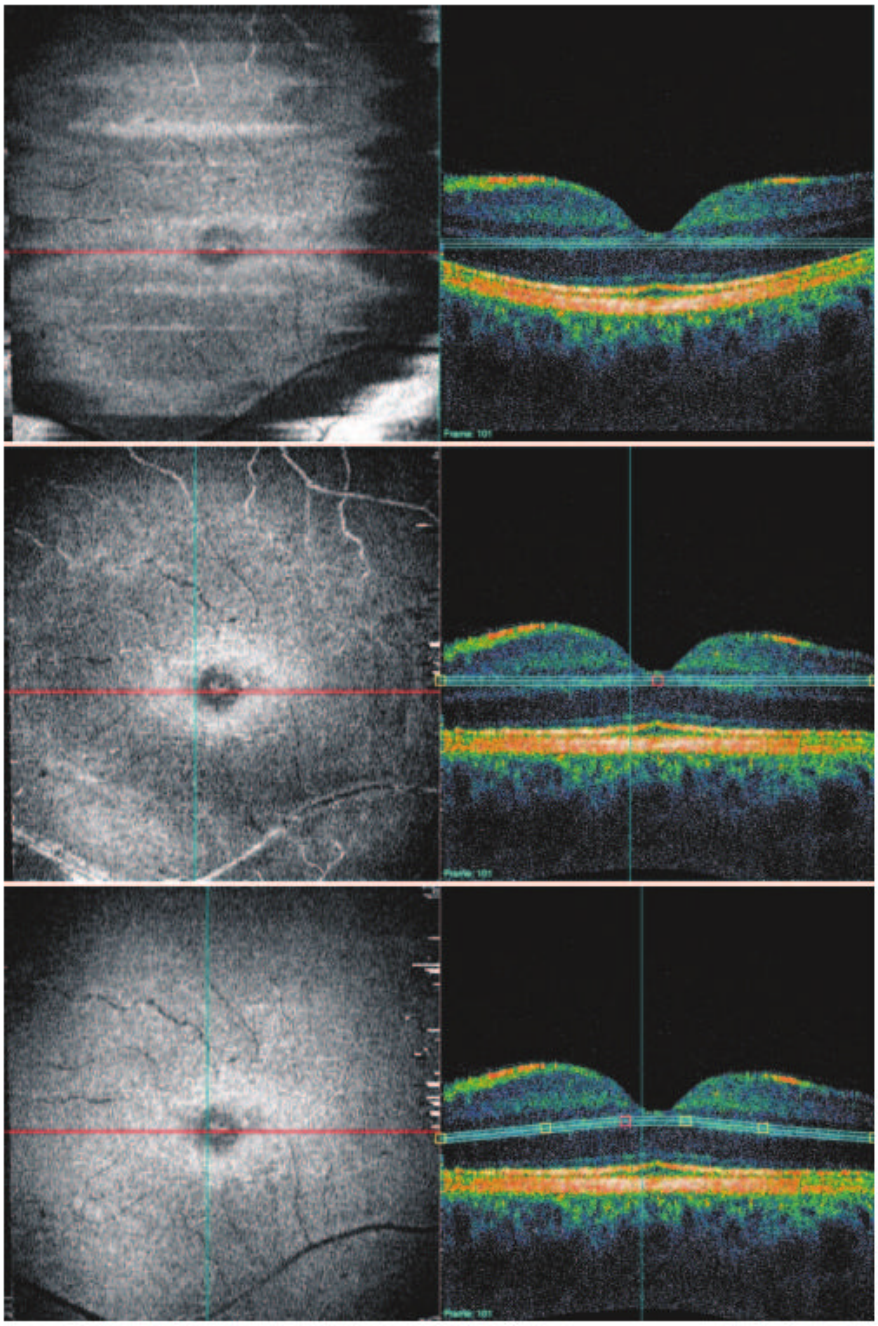

Figure 8.
RCN. Conventional C-mode (*top*) is marred by a mixture of multiple structures. Segmented C-mode (*middle*) shows the capillary network near the fovea, but other layers are visualized in the peripheral area. Contour-modeling C-mode (*bottom*) shows the most complete view of the RCN. This image was obtained with our prototype SD-OCT unit and was first flattened to the segmented RPE for both segmented and contour-modeling C-mode.

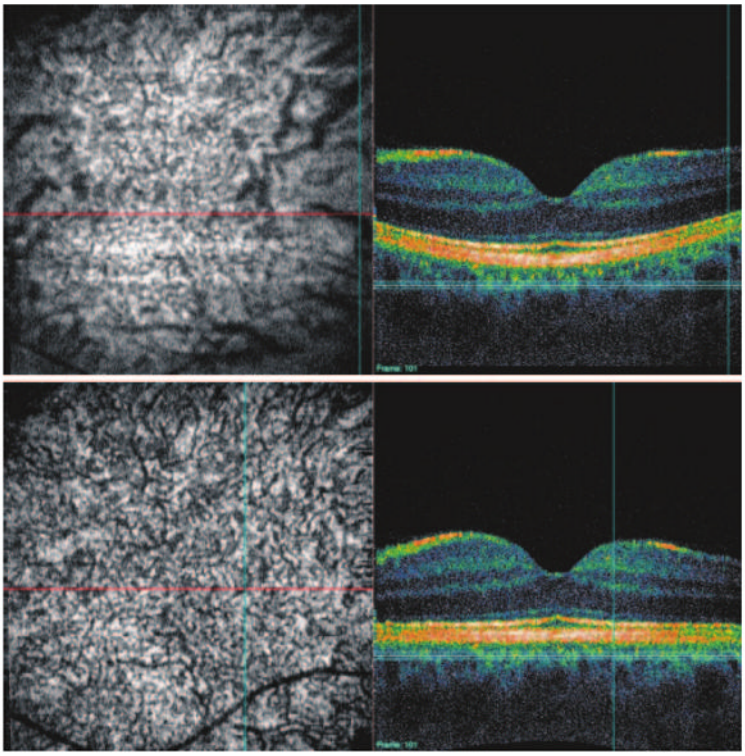

Figure 9.
CCN. Conventional C-mode (*top*) is marred by a mixture of multiple structures. Segmented and contour-modeling C-mode images (*bottom*) show the capillary network clearly. This image was obtained with our prototype SD-OCT unit and was first flattened to the segmented RPE for segmented and contour-modeling C-mode.

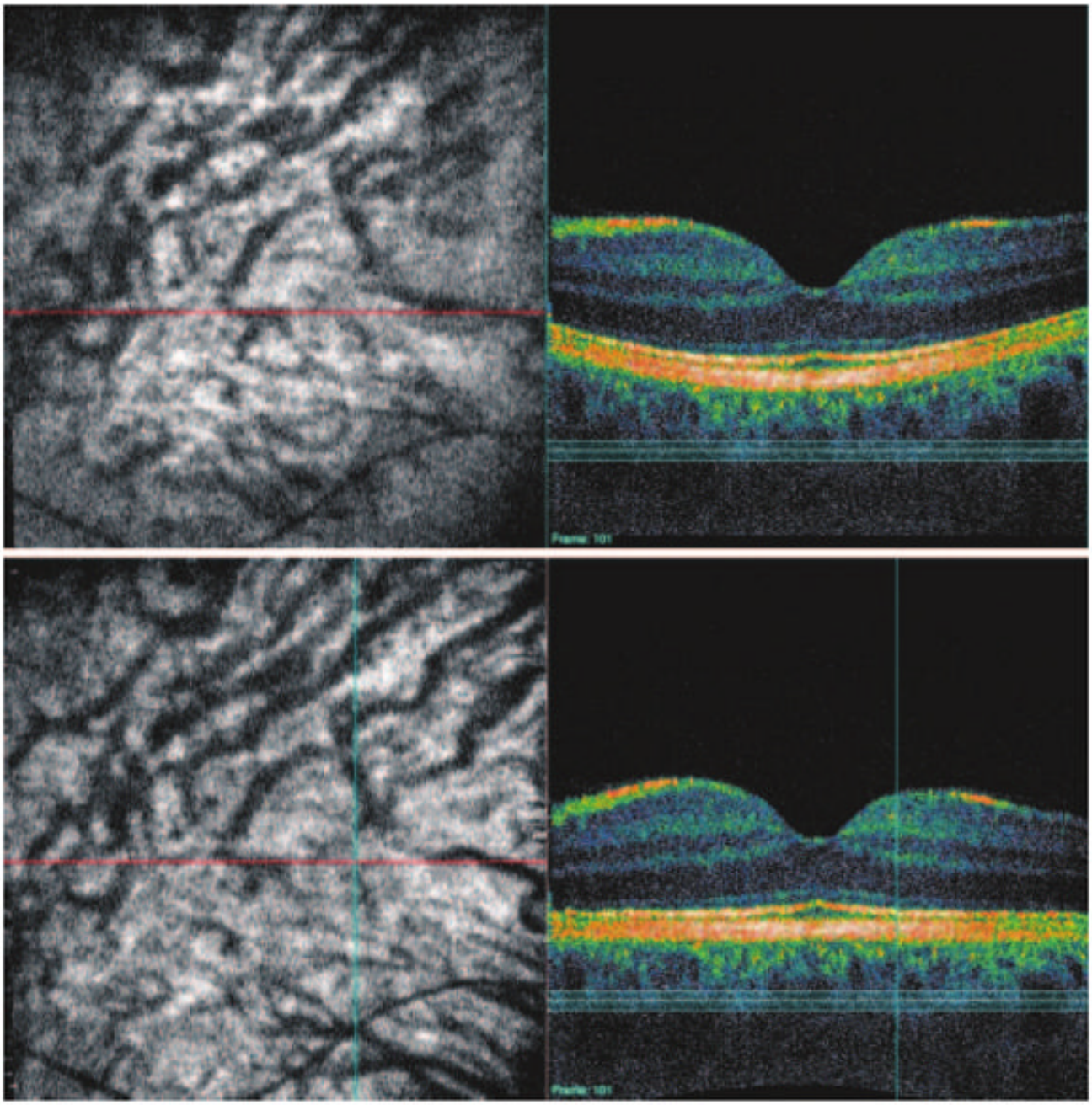

Figure 10.
CV. Conventional C-mode (*top*) shows CV in the central area but not in the peripheral area. Segmented and contour-modeling C-mode images (*bottom*) show CV clearly. This image was obtained with our prototype SD-OCT unit and was first flattened to the segmented RPE for segmented and contour-modeling C-mode.

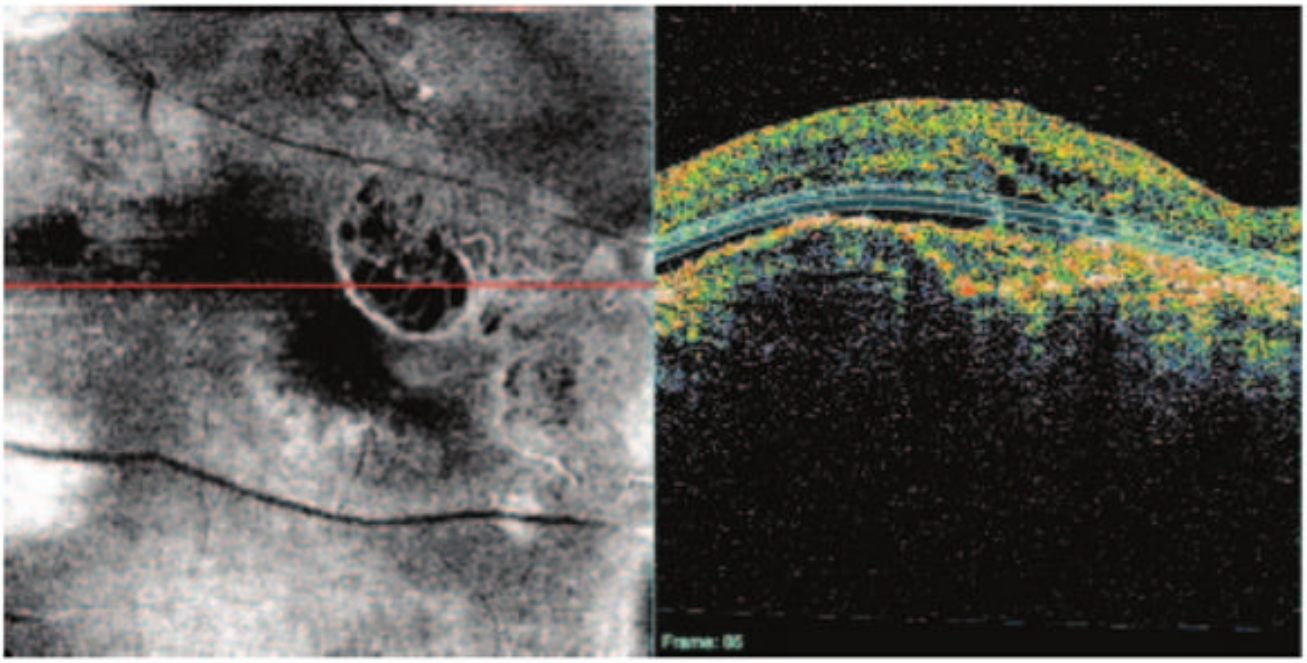

Figure 11.
Cystoid macular edema. Contour-modeling C-mode reveals the internal structure of the cystoid lesion associated with possible neovascular formation at the temporal side.

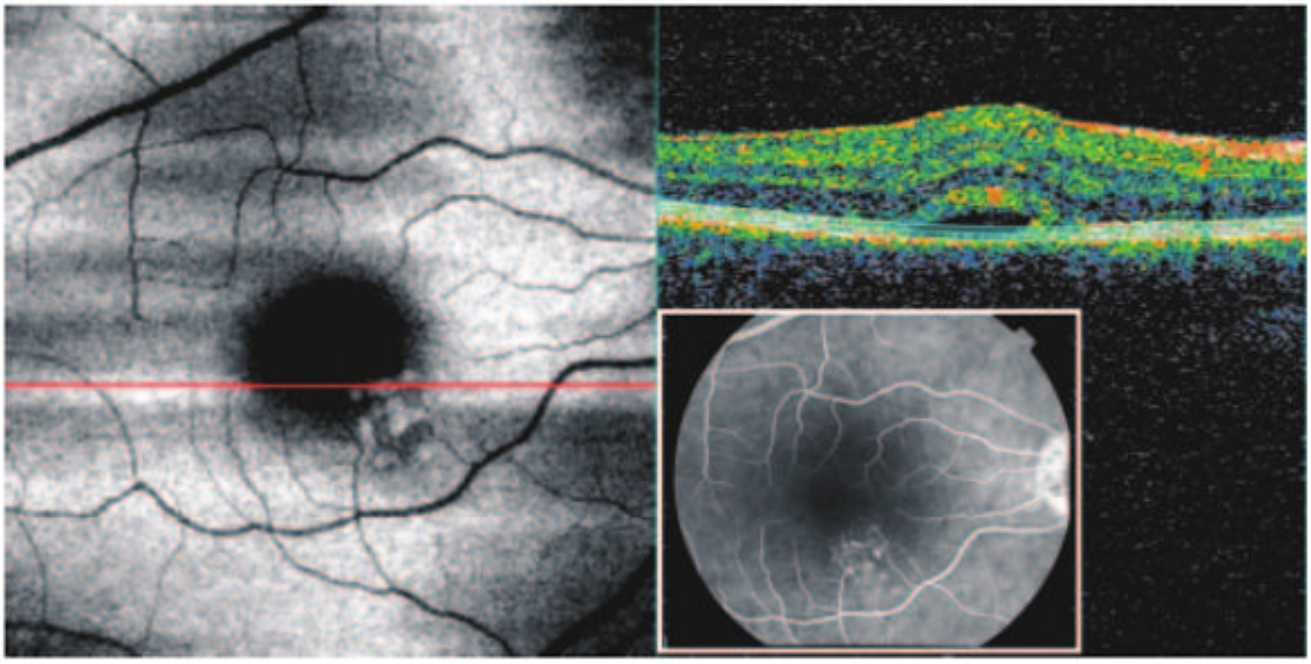

Figure 12.
CSR. Contour-modeling C-mode shows a serous detachment in the foveal region and a highly reflective structure inferior-nasal to the fovea, likely corresponding to the region of leakage as demonstrated on fluorescence angiography (FAG image, *inset*).

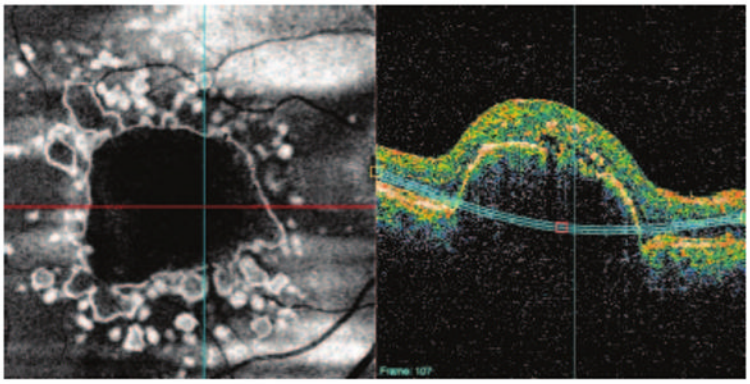

Figure 13.
ARMD. Contour-modeling C-mode shows clearly demarcated multiple drusen. Centrally, a drusenoid pigment epithelium detachment is found.

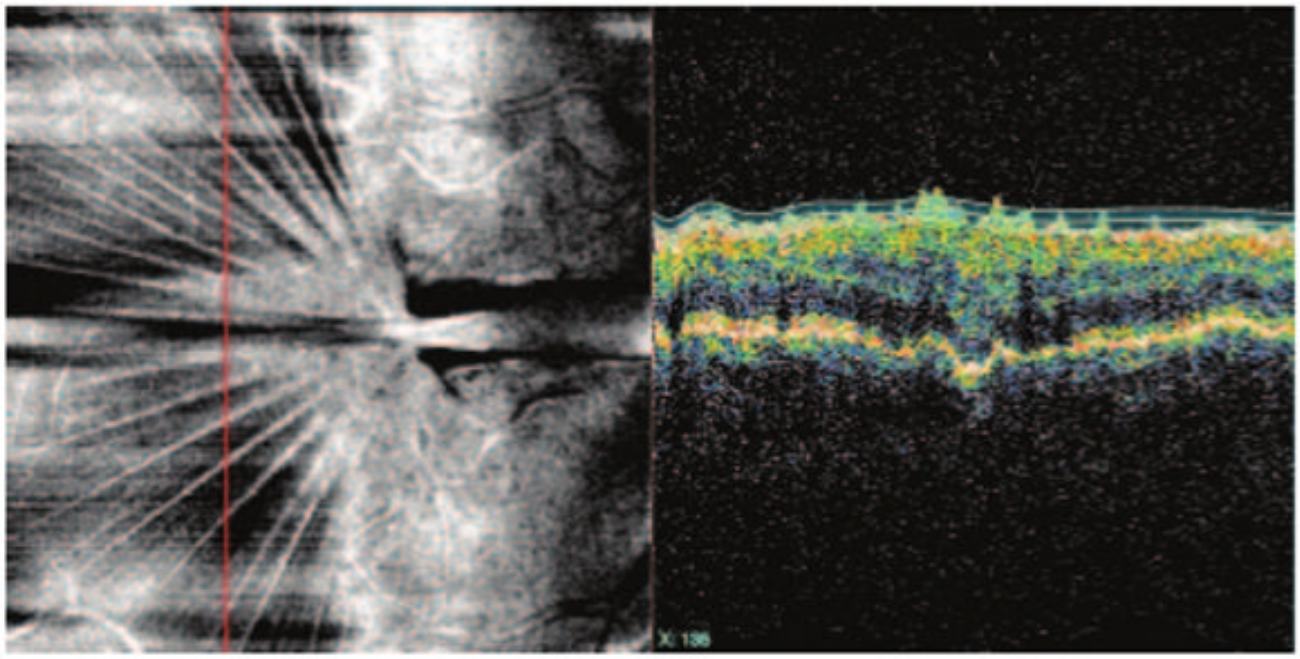

Figure 14.
Vitreoretinal traction secondary to an intraocular infection months earlier. Contour-modeling C-mode shows retinal folds at the ILM level centered at the point of greatest traction. Note that the cross-sectional OCT image (*right*) is sampled along the vertical line (*left, red line*) to visualize the retinal folds at the ILM level clearly.